Acta Materialia 168 (2019) 109–120

Contents lists available at ScienceDirect

Acta Materialia

journal homepage: www.elsevier.com/locate/actamat

Full length article

Thermodynamics of grain boundary segregation, interfacial spinodal and their relevance for nucleation during solid-solid phase transitions

A. Kwiatkowski da Silva*, R. Darvishi Kamachali, D. Ponge, B. Gault, J. Neugebauer, D. Raabe

Max-Planck-Institut für Eisenforschung, Max-Planck-Str. 1, 40237, Düsseldorf, Germany

ARTICLE INFO

Article history:
Received 25 September 2018
Received in revised form
5 February 2019
Accepted 5 February 2019
Available online 8 February 2019

Keywords:
Grain boundaries
Segregation
Nucleation
Embrittlement
Austenite reversion
Steels

ABSTRACT

Grain boundary segregation, embrittlement and phase nucleation are interconnected phenomena that are often treated separately, which is partly due to limitations of the current models to predict grain boundary segregation in non-ideal solid solutions. Here, a simple model is introduced to predict grain boundary segregation in solid solutions by coupling available bulk thermodynamic data with a mean-field description of the grain boundary character. The model is confronted with experimental results obtained in Fe-Mn alloys analysed by atom probe tomography. This model successfully predicts a first order transition or a discontinuous jump in the composition of the grain boundary which kinetically implies the formation of spinodal Mn fluctuations that tend to grow further with time within the segregated region. The increase in solute concentration at the grain boundary leads to an increase of the enthalpy of the boundary and to its embrittlement at lower temperatures. Once austenite is formed, the amount of segregated solute Mn on the grain boundaries is drastically reduced and the toughness of the grain boundary is increased.

© 2019 Acta Materialia Inc. Published by Elsevier Ltd. All rights reserved.

1. Introduction

Interfacial segregation or adsorption has been a perennial topic in materials and surface sciences for over a century. The first thermodynamic description of the problem dates back to J. W. Gibbs [1–3], who described interfaces having "phase-like" properties but with a zero thickness. Based on his model, Gibbs had proposed a relation between the changes in concentration of a component, when in contact with an interface, with the changes in interface energy. Langmuir proposed another model for surface adsorption [4], later adapted by McLean [5,6] to describe the segregation of solute elements to grain boundaries. The Langmuir-McLean adsorption isotherm describes both, bulk and grain boundaries as ideal solid solutions with non-interacting elements [7]. Fowler and Guggenheim [8] refined this model by considering that the interface behaves like a regular solution with interacting elements, thereby introducing the possibility to account for two-dimensional phase transitions within the confined volume of adsorbed layers [8–11]. This refinement appears reasonable when considering that the trend of solutes to segregate at interfaces often scales inversely with their bulk solubility, suggesting that non-ideal element interactions apply indeed for elements whose equilibrium segregation trend is high [6,12]. Regarding grain boundaries, the importance of such transitions was emphasized by e.g. Hart [9,13], Guttmann [14–17] and Cahn [18]. More recently, the term "complexion" was introduced in the literature to distinguish between the interfacial equilibrium state and the bulk equilibrium state (phase) [19–22]. In this context, complexion transitions (or interface transitions) are the result of a discontinuity of the first- or higher-order derivative of the interface energy as a function of one of the interfacial thermodynamic parameters [22–24].

Interfacial adsorption or segregation transitions strongly influence the properties of interfaces. Solute segregation to grain boundaries has been widely associated with grain boundary embrittlement [9,14,21,22,25–28], phase nucleation [25,29–35], abnormal grain growth [22,36,37] and stabilization of nanocrystalline materials [37–48]. In many of these applications that make use of the adsorption isotherm for microstructure design, the segregating solutes are assumed to behave as an ideal solution when decorating grain boundaries, i.e. they follow the McLean isotherm. In contrast to this picture, we recently reported observations of confined spinodal fluctuations at crystalline defects [29].

* Corresponding author.
E-mail address: a.kwdasilva@mpie.de (A. Kwiatkowski da Silva).

https://doi.org/10.1016/j.actamat.2019.02.005
1359-6454/© 2019 Acta Materialia Inc. Published by Elsevier Ltd. All rights reserved.

These spinodal fluctuations, observed in a Fe-9 at.%Mn alloy, grow in composition and wavelength with time and might be a precursor pathway for the formation of the first nucleus of austenite. After austenite is formed and in local equilibrium with the surrounding bulk BCC matrix phase, the fluctuations and the strong segregation vanish, clearly indicating that they are *metastable* precursor fluctuations. After formation of the locally stable phase at the interface, here austenite, the formerly segregated atoms partition into it, leaving a less decorated interface behind.

Here, a model is introduced and applied to predict the grain boundary segregation and phase state behaviour of substitutional solid solutions by coupling Calphad thermodynamic data originally derived for bulk phases with a mean-field description of the grain boundary. The approach is largely inspired by models previously developed by Guttmann [14–17], Wynblatt [20,49,50] and other authors [6,12,21,51,68]. The concept is first described for regular solid solutions and later extended to magnetic solid solutions which are exemplified here by the Fe-Mn binary alloy. It is shown that this approach provides the opportunity for a more consistent thermodynamic description of the spinodal segregation, grain boundary embrittlement and austenite reversion in this alloy. The model successfully predicts the existence of a first order transition of the interface for Fe-Mn BCC grain boundaries which was experimentally validated by atom probe tomography (APT).

2. The regular solution model of grain boundary segregation

Let us first assume that both, the bulk (b) and the grain boundary (gb), are binary regular solutions at a given temperature (T):

$$G^{b} = H^{b} - TS^{b} = X_A^{b}\,{}^0G_A^{b} + X_B^{b}\,{}^0G_B^{b} + \Delta H_{mix}^{b} - T\Delta S_{mix}^{b} \tag{1}$$

$$G^{gb} = H^{gb} - TS^{gb} = X_A^{gb}\,{}^0G_A^{gb} + X_B^{gb}\,{}^0G_B^{gb} + \Delta H_{mix}^{gb} - T\Delta S_{mix}^{gb} \tag{2}$$

where G, H and S are, respectively, molar Gibbs free-energy, enthalpy and entropy of the bulk (b) or grain boundary (gb). X_i and ${}^0G_i$ are the molar fraction and the Gibbs free-energy of the bulk (b) or grain-boundary (gb) of the pure component *i* (A and B), respectively, with $X_A + X_B = 1$ mol. The only excess term in a regular solution is the molar enthalpy of mixing (ΔH_{mix}) that is given by:

$$\Delta H_{mix} = \alpha_{AB} X_A X_B \tag{3}$$

where α_{AB} is the regular solution parameter [52]. Assuming steady state diffusional equilibrium between the bulk and grain boundary, the (relative) chemical potentials of the components in the bulk ($\delta\mu^b = \mu_B^b - \mu_A^b$) and grain boundary ($\delta\mu^{gb} = \mu_B^{gb} - \mu_A^{gb}$) should be equal:

$$\begin{aligned}\delta\mu^b &= \left(\frac{\partial G^b}{\partial N_B^b}\right)_{p,T,N_B} - \left(\frac{\partial G^b}{\partial N_A^b}\right)_{p,T,N_A} = \delta\mu^{gb} \\ &= \left(\frac{\partial G^{gb}}{\partial N_B^{gb}}\right)_{p,T,N_B} - \left(\frac{\partial G^{gb}}{\partial N_A^{gb}}\right)_{p,T,N_A}\end{aligned} \tag{4}$$

which is equivalent to a parallel tangent construction between the molar free energy curves of the bulk and the grain boundary [53]. Therefore, we can write:

$$\frac{dG^b}{dX_B^b} = \frac{d^0G^b}{dX_B^b} + \frac{dG_{mix}^b}{dX_B^b} = \frac{dG^{gb}}{dX_B^{gb}} = \frac{d^0G^{gb}}{dX_B^{gb}} + \frac{dG_{mix}^{gb}}{dX_B^{gb}} \tag{5}$$

The above expression (5) can be rearranged into the Fowler-Guggenheim isotherm [8,48,54]:

$$\frac{X_B^{gb}}{1-X_B^{gb}} = \frac{X_B^b}{1-X_B^b} exp\left[-\frac{\Delta G_0^{seg} + \alpha_{AB}^{gb} - \alpha_{AB}^{b} - 2\left(\alpha_{AB}^{gb}X_B^{gb} - \alpha_{AB}^{b}X_B^{b}\right)}{RT}\right] \tag{6}$$

with

$$\Delta G_0^{seg} = \Delta^0 G^{gb} - \Delta^0 G^{b} \tag{7}$$

which is equivalent to the difference in grain boundary energy of the pure components with $\Delta^0 G^b = {}^0G_A^b - {}^0G_B^b$ and $\Delta^0 G^{gb} = {}^0G_A^{gb} - {}^0G_B^{gb}$. ΔG_0^{seg} expresses the difference in the bulk and grain boundary environments for the pure components. For non-interacting solutes ($\alpha = 0$), the above isotherm formulation reduces to the McLean isotherm [5,7]. Furthermore, the model predicts that segregation could occur even for negative values of the ideal segregation Gibbs energy ΔG_0^{seg}, but it will only occur if the total energy of segregation ΔG^{seg} is negative, which is equal to $\Delta G^{seg} = \Delta G_0^{seg} + \alpha_{AB}^{gb} - \alpha_{AB}^{b} - 2(\alpha_{AB}^{gb}X_B^{gb} - \alpha_{AB}^{b}X_B^{b})$ in the Fowler-Guggenheim model.

3. Mean-field interpretation of segregation in regular solution alloys

Assuming first-order neighbour interaction among the atoms, the regular solution parameter in a binary A-B solution is given as [52]:

$$\alpha_{AB} = z\left[\varepsilon_{AB} - \frac{\varepsilon_{AA} + \varepsilon_{BB}}{2}\right] = z\omega_{AB}, \tag{8}$$

where z is the coordination number, ε_{AB}, ε_{AA} and ε_{BB} are the A-B, A-A and B-B interaction energies, respectively, and ω_{AB} is the average interaction energy. Positive values of ω_{AB} indicate a trend towards demixing of elements A and B. It is possible to write the enthalpy of mixing as a function of these parameters for the bulk and for the grain boundary:

$$\Delta H_{mix}^{b} = \alpha_{AB}^{b} X_A^{b} X_B^{b} = z^{b}\omega_{AB}^{b} X_A^{b} X_B^{b} \tag{9}$$

$$\Delta H_{mix}^{gb} = \alpha_{AB}^{gb} X_A^{gb} X_B^{gb} = z^{gb}\omega_{AB}^{gb} X_A^{gb} X_B^{gb} \tag{10}$$

If we assume that the average interaction energy ω_{AB} is the same (or better, sufficiently similar) for the bulk and the grain boundary solutions, $\omega_{AB}^{b} = \omega_{AB}^{gb}$, the only parameter left to express the difference between the bulk and grain boundary is the coordination number, z, which describes the local lattice structure in each environment. Hence, we propose to describe the enthalpy of mixing of the grain boundary solution (ΔH_{mix}^{gb}) with a given composition as a function of the coordination number and the enthalpy of mixing of the bulk with the same composition:

$$\Delta H_{mix}^{gb} \cong \frac{z^{gb}}{z^{b}} \Delta H_{mix}^{b} \tag{11}$$

Such an approach could be described as a "bond cutting model" because the average bonding energies are here assumed to be the same, independent of the coordination number. This assumption has the limitation of ignoring the increase in bond strength with decreasing coordination number [55], but it is used here as a first approximation that can be improved in future work. For

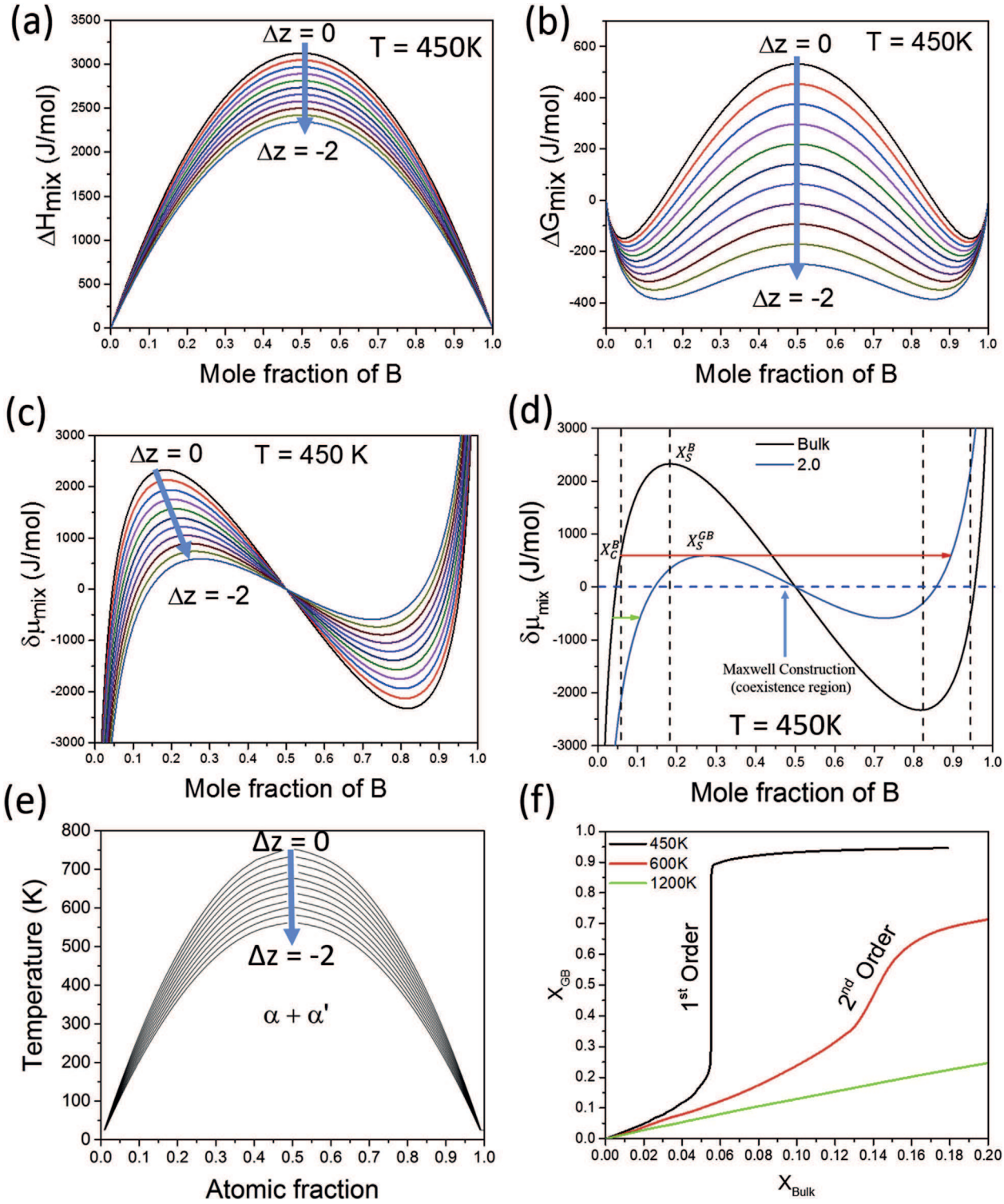

Fig. 1. Effect of the reduction in coordination (Δz) of a hypothetical solid solution assuming a regular solution parameter equal to 12500 J/mol and the coordination number of the bulk equals to 8 (for an assumed BCC phase). In all figures Δz = 0 refers to the full lattice coordination that atoms have in the bulk and Δz = −2 refers to reduced coordination such as encountered in the grain boundary. The approach suggested here assumes a "bond cutting" model because the average bonding energies remain unchanged, independent of the coordination number. This assumption has the limitation of ignoring the increase in bond strength with decreasing coordination number (a) Enthalpy of mixing in function of the mole fraction of solute B for different coordination shifts. (b) Gibbs energy of mixing at 450 K in function of the mole fraction of solute B for different coordination shifts. (c) First derivative of the Gibbs energy of mixing at 450 K in function of the mole fraction of solute B for different coordination shifts. (d) Chemical potential of the bulk and the grain boundary. For any composition below X_C^B, adsorption or segregation will occur chemically homogeneously and compositional variations in the segregated area will be due to topological effects only. For any composition between X_C^B and the critical point (spinodal) of the bulk X_S^B, confined spinodal fluctuations will happen for the here assumed hypothetical regular solution alloy at the interface in addition to the compositional variations due to the structure of the grain boundary. (e) Chemical spinodal for different temperatures, composition and atomic fraction of solute for the hypothetical solid solution. (f) Equilibrium composition of a grain boundary with −2 coordination shift (i.e. z = 6) in metastable local equilibrium with an infinitely large bulk with a coordination number of z = 8 for the BCC lattice case.

convenience, the average grain boundary coordination shift (Δz) is defined as the difference between the average grain boundary coordination (z^{gb}) and the bulk (z^{b}) coordination:

$$\Delta z = z^{gb} - z^{b} \tag{12}$$

Considering the non-coherent atomistic structure of the grain boundary, the averaged coordination number z^{gb} is expected to be smaller than the corresponding number in the bulk and, therefore, $\Delta z \leq 0$. The consequences of this mean-field approximation of the thermodynamic description of a grain boundary is visualized for a hypothetical regular solution described by Eqs. (1), (2) and (11) in Fig. 1. Fig. 1a shows the effect of the reduction in coordination number on the enthalpy of mixing of a hypothetical solid solution of A and B atoms with positive enthalpy of mixing. A lower coordination number implies the reduction of the enthalpy of mixing of the solution and, as a consequence, the reduction of the total mixing free energy of the solution. Fig. 1b illustrates the effect of the reduction of coordination number on the Gibbs free-energy of mixing of the solution at a given temperature. Clearly, regions of higher coordination will tend to partition solutes to regions of lower coordination (lower free energy of mixing).

Fig. 1c and d displays the effect of the reduction of coordination number on the first derivative of the free energy of mixing of the system (relative chemical potentials). At lower temperatures (e.g. 450 K in this case), the first derivative presents a maximum and minimum for the chosen hypothetical regular solution (chemical spinodal points for the strain-free state) where $d^2G_{mix}/dX^2 = 0$. The reduction of the coordination number for atoms inside the grain boundary results in new free energy and chemical potential curves such that the equilibrium partitioning concentrations are shifted along the concentration axis (x axis) and towards the centre between the corresponding bulk values. Furthermore, it is clear that the magnitude of upper (and lower) chemical potentials for spinodal decomposition, $\delta\mu^{gb,s}$, reduces as z^{gb} decreases, indicating a lower spinodal barrier inside the grain boundary. Fig. 1e shows the effect of the reduction of coordination number on the chemical spinodal of this hypothetical solid solution. Fig. 1f shows the composition of the hypothetical grain boundary with a −2 coordination shift in metastable local equilibrium with a given bulk composition. For this hypothetical solution, at 450 K, the grain boundary will display a first order transition or spinodal segregation. At 600 K, the grain boundary will display a second order transition. At 1200 K, the grain boundary segregation will exhibit a close to linear behaviour for this hypothetical regular solution.

When the chemical potential of the bulk ($\delta\mu^{bulk}$) is equal or higher than that of the spinodal point of the interface ($\delta\mu^{gb,s}$), spontaneous spinodal fluctuations at the grain boundary become possible. Therefore, the critical composition of the bulk (X_C^B) for the spinodal fluctuation to occur in the grain boundary can be obtained by:

$$\delta\mu_C^{bulk} = \frac{dG^b}{dX_C^B} = \delta\mu^{gb,s} = \frac{dG^{gb}}{dX_s^{GB}} \tag{13}$$

This is schematically represented in Fig. 1d which shows the chemical potential of the bulk and of the grain boundary. For the chosen solution any composition below X_C^B, adsorption or segregation will occur homogeneously and compositional variations in the segregated area will be due to specific topological grain boundary structure effects only. For any composition between X_C^B and the critical point (spinodal) of the bulk X_S^B, confined spinodal fluctuations occur at the interface in addition to possible compositional variations due to the structure of the grain boundary. The final state marks a first order transition of the interface. These confined spinodal fluctuations at the grain boundary are due to the new chemical working point that is reached on the interface but not necessarily in the adjacent bulk. The solute-rich regions of these confined spinodal fluctuations can act as precursor states to the nucleation of a new phase when they become strong enough in composition and wavelength. This is a sequence which is analogous to spinodal decompositions known from the bulk, such as the Al-Cu system, where the required random composition fluctuations that are required to reach the composition of the stable phase become lower with increasing spinodal precursor amplitude. This effect sheds new light on the heterogeneous nucleation mechanism which is usually associated only with the advantage of interface energy provided by the grain boundary. The new model shows that heterogeneous nucleation at interfaces can be also promoted by spinodal composition enrichment, i.e. precursor states at the grain boundary which do not necessarily occur in the adjacent bulk. This means that a grain boundary can assist nucleation in a twofold manner, through its available interface portion and through its interface-specific chemical working point which may enable phase precursors not found in the bulk.

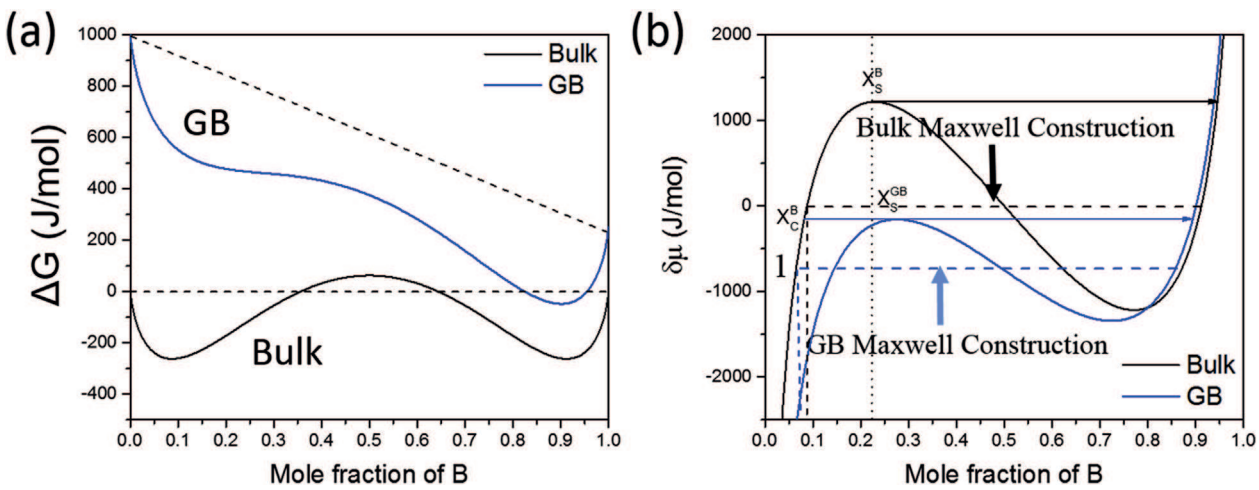

Fig. 2. Free energies (a) and chemical potentials (b) of the grain boundary (z = 6) compared to its corresponding bulk (z = 8 for BCC) assuming $\Delta G^{seg} = +1000 - 500X_A$ [J/mole]. The introduction of ΔG^{seg} enables the possibility of a first order grain boundary transition below the solubility limit of the bulk miscibility gap by shifting the grain boundary Maxwell construction vertically relative to the bulk Maxwell construction.

Fig. 1d reveals that, although X_C^B is strongly lowered by reducing the average coordination, the coexistence region (given by the Maxwell construction) remains the same and is hence independent of the coordination number. This results implies, that under such constraints, the spinodal fluctuations at the grain boundary can be obtained only for compositions inside the two-phase region of the bulk phase diagram (although for compositions outside the grain boundary spinodal region). These confined spinodal fluctuations might act as a pathway for the nucleation of the α' (B-rich) phase, but they will not occur below the solubility limit and evolve to a stable segregation composition. In order to introduce such possibility and to resolve the full picture of the grain boundary segregation problem, we now discuss a hypothetical grain boundary characterized by a reduced coordination number $\Delta z = -2$ relative to the adjacent BCC bulk matrix in the presence of the intrinsic (ideal) segregation energy assumed to be $\Delta G_0^{seg} = +1000 - 500X_A$ [J/mole]. Fig. 2a and b shows the free energies and chemical potentials of the grain boundary (z = 6) compared to its

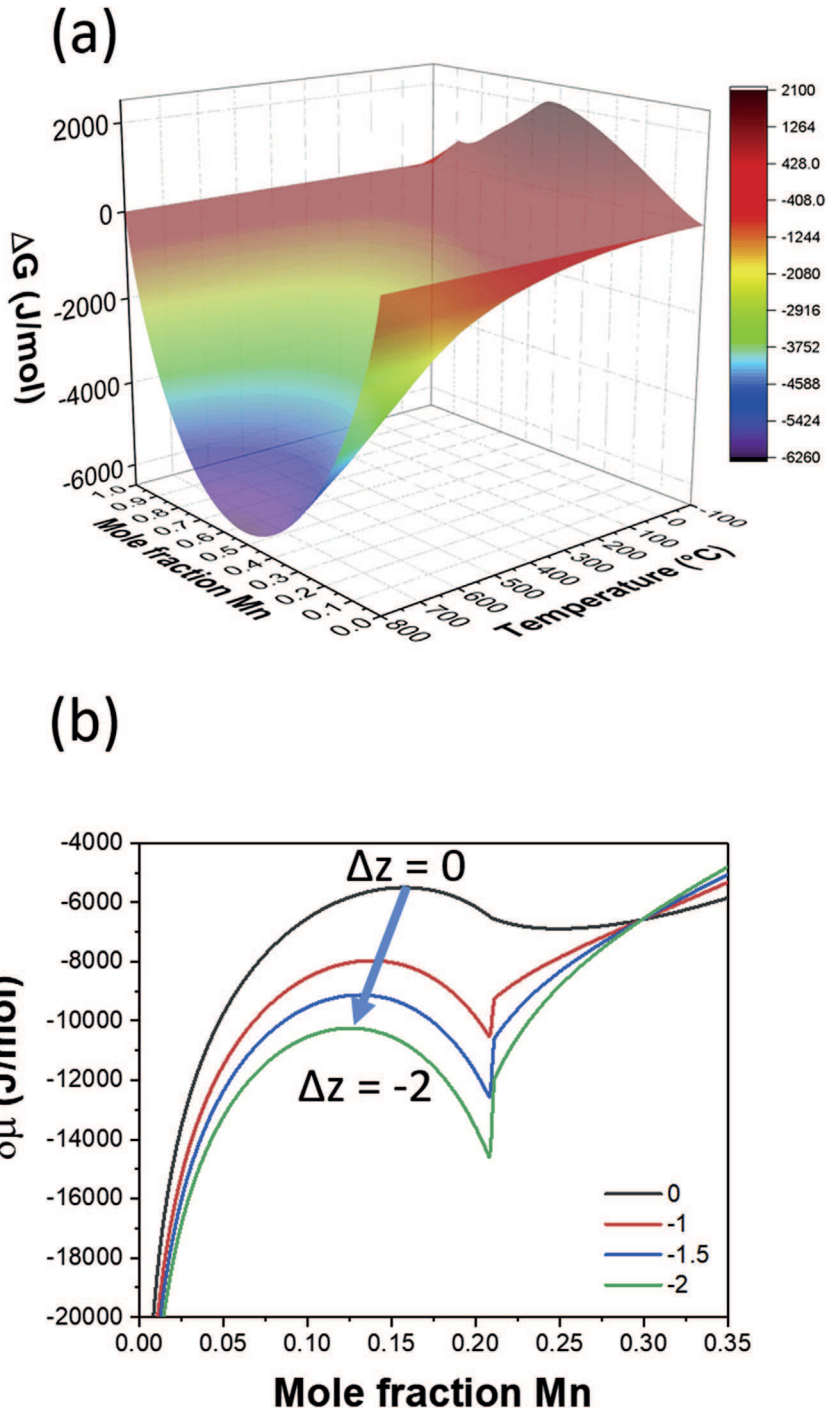

Fig. 3. (a) Gibbs energy of mixing (including magnetism) of Fe and Mn for the BCC phase with a coordination number of z = 8. (b) Dependence of the first derivative of the Gibbs energy of mixing at 450 °C (including magnetism) of Fe and Mn for the BCC phase (z = 8) in function of the coordination number shift, indicating the reduced number of nearest neighbour bonds characteristic of grain boundaries.

corresponding bulk (z = 8 for the BCC lattice), respectively. Comparing to Fig. 1b and c shows that an asymmetric change in the free energy and a vertical shift in the chemical potential result from a nonzero ideal segregation energy ($\Delta G_0^{seg} \neq 0$). The equilibrium concentrations (Maxwell construction) are shown in Fig. 2b. At point 1, a first order transition in the grain boundary occurs, in which a two-phase grain boundary state (z = 6) is in equilibrium with the single-phase (homogeneous) bulk state (z = 8). While below this point segregation in the grain boundary occurs homogeneously, at this point a sharp jump in the grain boundary concentration is expected. However, for a regular solution with a symmetric miscibility gap, a very high absolute value of ΔG_0^{seg} is necessary in order to obtain a first order transition, i.e. a transition from low to high segregation and spinodal segregation (X_C^B) of the grain boundary at compositions significantly below the solubility limit of the bulk. In the following, we will show that such a situation is different for asymmetric miscibility gaps that can arise due to other energy contributions such as for instance caused by magnetic energy terms.

4. Solid solutions with magnetic contributions

Similar to the mixing enthalpy, a magnetic energy contribution can also strongly depend on the coordination number z. The Inden-

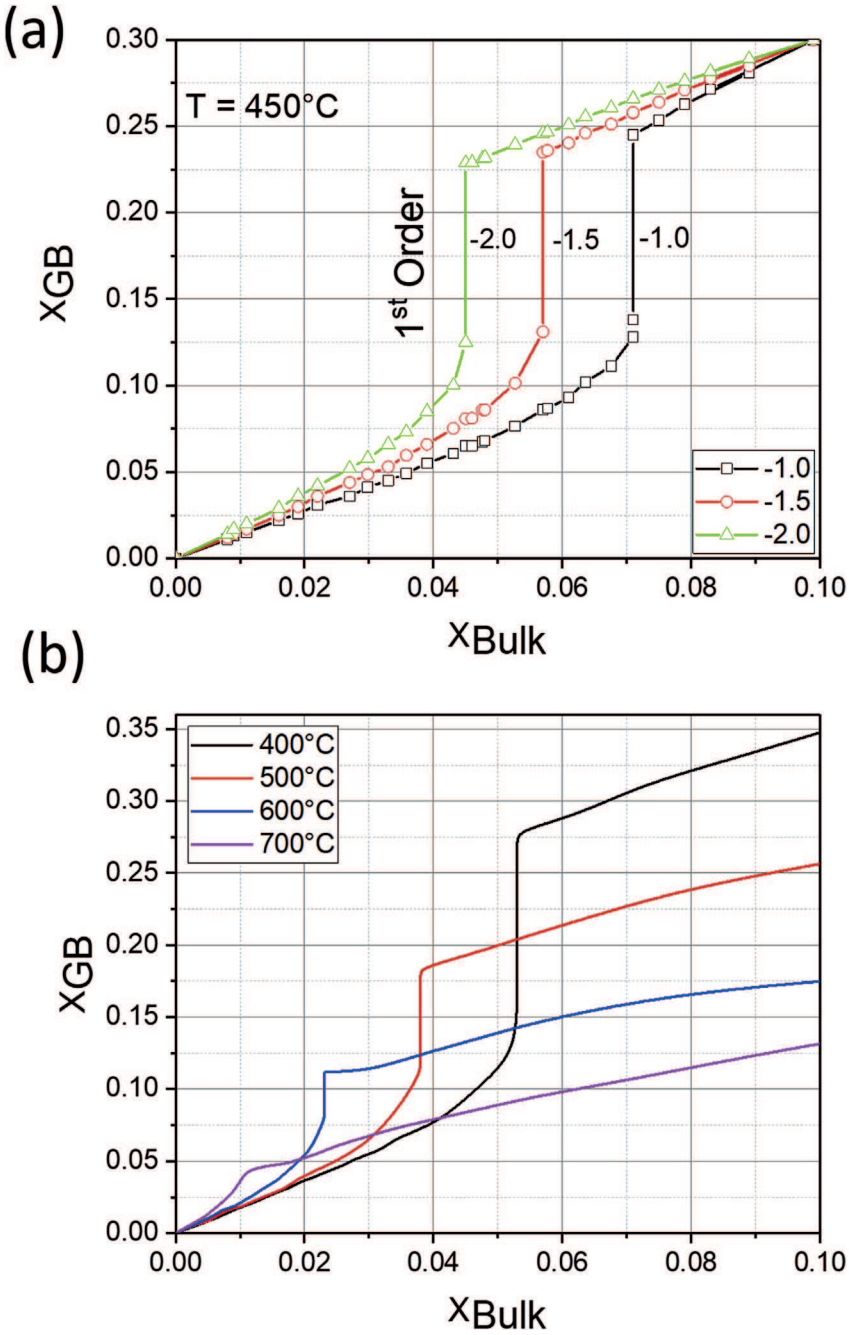

Fig. 4. Segregation isotherms assuming metastable local diffusional equilibrium between the BCC bulk phase (coordination number z = 8) and the grain boundary (reduced coordination number z = 6). (a) Segregation isotherms at 450 °C assuming different coordination shifts for the grain boundary. (b) Segregation isotherms at different temperatures assuming a grain boundary with a coordination shift of −2.0.

Hillert-Jarl formalism [56–61] is the basis for most of the functions that incorporate magnetic ordering contributions in Calphad databases. From the heat capacity, the magnetic contribution ${}^{mg}G_m^{\alpha}$ to the Gibbs free energy can be obtained:

$$ {}^{mg}G_m^{\alpha} = -RTln(\beta+1)f(\tau) \tag{14} $$

where β is the mean magnetic moment per mole of formula unit, $f(\tau)$ is a function of $\tau = T/T_c$ and T_c is the Curie temperature. The values of magnetic enthalpy and entropy can be obtained by expressions available in the literature or directly from a Calphad database. While Equation (14) decomposes in complex forms of enthalpy and entropic contributions, the dependency of the molar magnetic enthalpy, H_{mag}, on the coordination number can be demonstrated using a pairwise interactions model (Bragg-Williams-Gorsky approximation) [58]:

$$ H_{mag} = \frac{1}{2}\sum_k z^{(k)} J^{(k)} \sigma^2 \tag{15} $$

where the summation goes over the different neighbouring shells (k, = 1, 2, …), $z^{(k)}$ is the coordination number, $J^{(k)}$ describes the molar interaction energy, and σ is the mean spin value per atom. Following this model, a similar mean-field approximation to the magnetic excess enthalpy ΔH_{mag} is proposed here as it was adopted above for the enthalpy of mixing. In this context, we assume that the magnetic excess enthalpy of the grain boundary ΔH_{mag}^{gb} can be approximated from the magnetic excess enthalpy of the bulk ΔH_{mag}^{b} with a linear dependency on the coordination number that results. Therefore, the excess enthalpy of the grain boundary ΔH_{xs}^{gb} can be approximated from the excess enthalpy of the bulk ΔH_{xs}^{gb}:

$$ \Delta H_{xs}^{gb} = \Delta H_{mix}^{gb} + \Delta H_{mag}^{gb} \cong \frac{z^{gb}}{z^{b}}\Delta H_{mix}^{b} + \frac{z^{gb}}{z^{b}}\Delta H_{mag}^{b} = \frac{z^{gb}}{z^{b}}\Delta H_{xs}^{b} \tag{16} $$

Due to the asymmetry of the ΔH_{mag} in compositional space, the vertical shifts in chemical potentials (and corresponding Maxwell constructions) can be achieved even if $\Delta G_0^{seg} = 0$.

5. Binary Fe-Mn alloys

Using these mean-field approximations we are now able to describe grain boundary segregation using available bulk thermodynamics. The free energies and enthalpies of mixing (including

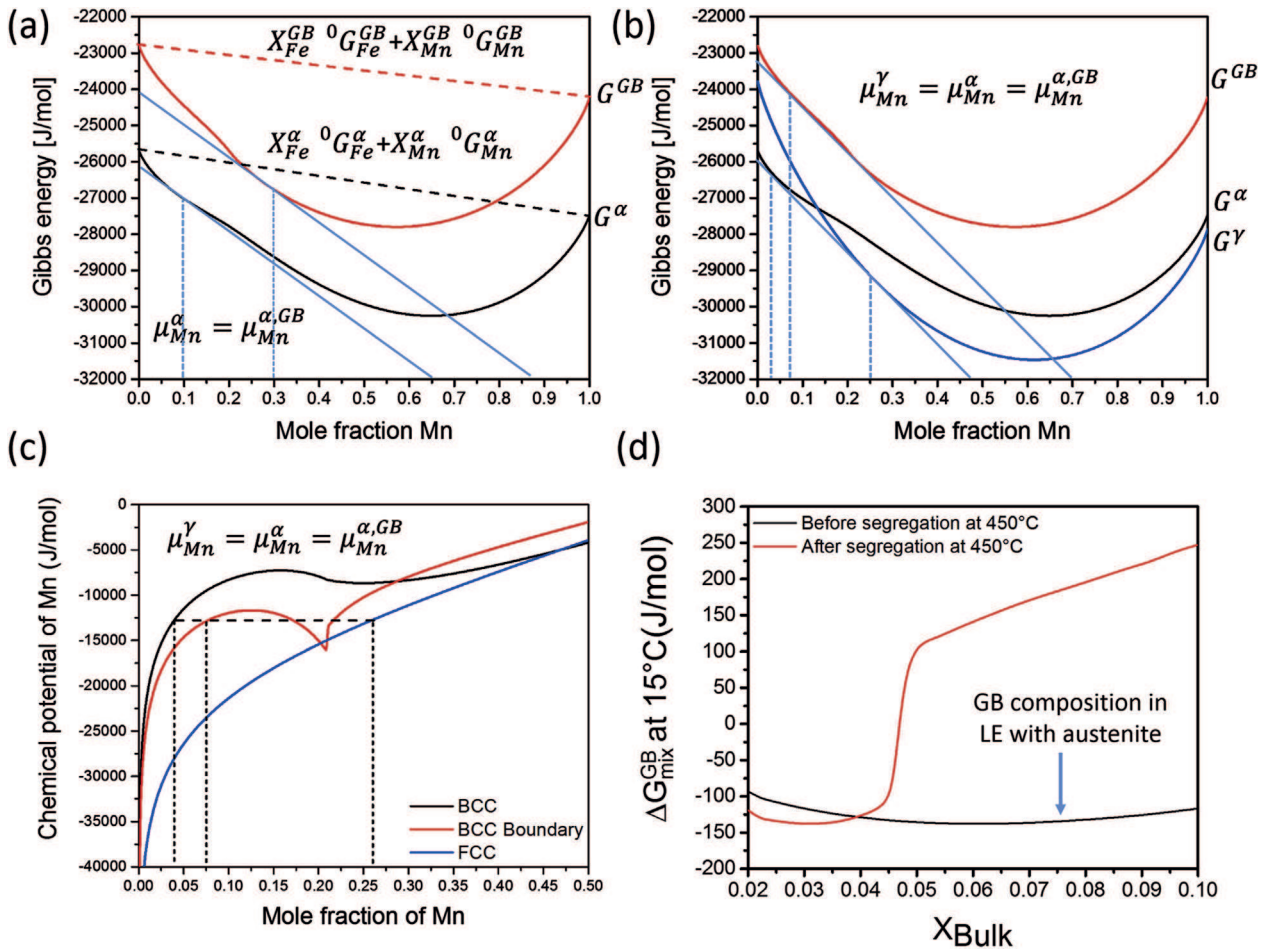

Fig. 5. Graphical representation of the calculation of equilibrium composition of the grain boundary, characterized by reduced coordination of z = 6, (segregation/adsorption) by the parallel tangent construction: (a) Equilibrium composition of the grain boundary before the formation of austenite represented using Gibbs Free-energies. (b) Equilibrium composition of the grain boundary after the formation of austenite represented using Gibbs free-energies. (c) Equilibrium composition of the grain boundary after the formation of austenite represented using chemical potentials. (d) Grain boundary energy of mixing at 15 °C (including magnetism) before and after segregation at 450 °C. The spinodal segregation drastically increases the grain boundary energy at lower temperatures and the formation of austenite leads to a decrease of this energy. GB: grain boundary; LE: local equilibrium. Grain boundary coordination z = 6; BCC matrix coordination z = 8.

magnetic effect) for the FeMn system (bulk phases) are extracted from ThermoCalc using the TCFE9 database. Details of the models and data used in this database can be found in Refs. [62,63]. For simplicity, the intrinsic (ideal) segregation Gibbs energy will be assumed to be zero ($\Delta G_0^{seg} = 0$). Fig. 3a shows the Gibbs energy of mixing (including magnetism) of Fe and Mn for the BCC phase with a coordination of z = 8 as a function of temperature. In this alloy system, the asymmetric dependence of the magnetic enthalpy with Mn composition leads to the asymmetry in the Gibbs free energy. Fig. 3b shows the dependence of the chemical potentials at 450 °C (including magnetism) of Fe and Mn for the BCC phase as a function of the coordination number shift (Δz). At a given temperature, segregation (diffusion) will take place from the bulk (z = 8) to regions of lower coordination such as grain boundaries (z < 8). Fig. 4a and b shows segregation isotherms obtained assuming metastable local equilibrium between the BCC bulk phase and the grain boundary. The isotherms show the grain boundary composition (X_{GB}) in local equilibrium with a given bulk composition (X_{Bulk}). The grain boundary composition at which the first order transition takes place marks the spinodal point of the grain boundary (X_S^{GB}). Fig. 4a shows segregation isotherms at 450 °C assuming different coordination shifts for the grain boundary. The critical bulk composition at which the first order transition takes place is decreased by decreasing the average coordination number. Above the critical composition, the interaction between the solutes starts to be stronger than the energy difference between sites with different coordination. Fig. 4b shows segregation isotherms at different temperatures assuming a grain boundary with a coordination shift of $\Delta z =$ -2 relative to the BCC lattice (z = 8). The total amount of segregation (grain boundary composition) is

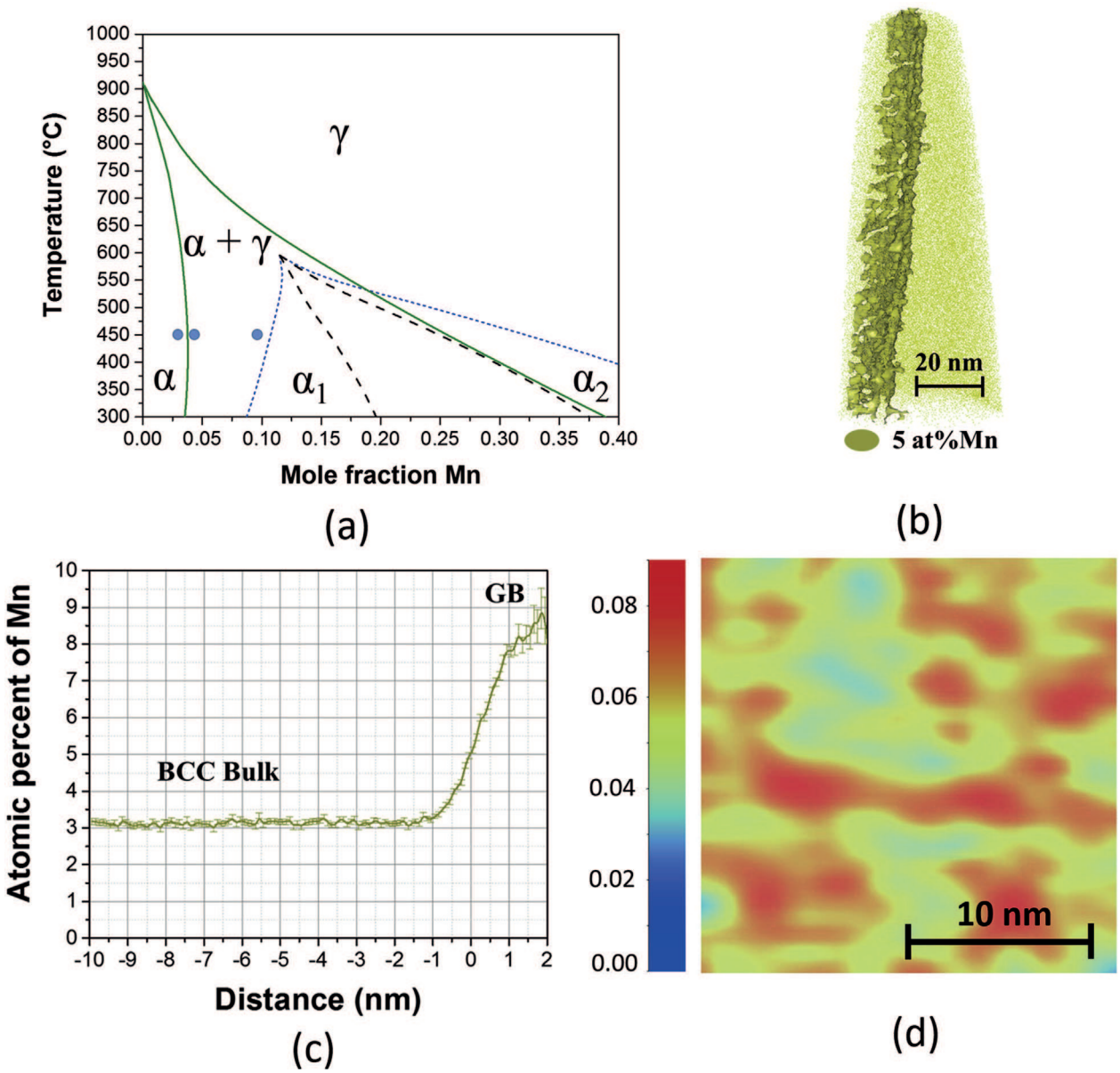

Fig. 6. (a) The Fe-Mn phase diagram (calculated using the Thermocalc software in conjunction with the TCFE7 database) including the metastable magnetic miscibility gap (dashed blue lines) and magnetic spinodal (dashed black lines) of the BCC phase. The blue points indicate the composition of the alloys probed during this study. APT analysis: Fe-3Mn (at.%) solid solution bulk alloy, 50% cold-rolled and subsequently annealed at 450 °C for 2 months. (b) APT reconstruction: 5 at% Mn isosurface revealing a grain boundary. (c) Proxigram obtained from the isosurfaces displayed in (b). (d) In-plane 2D compositional map of Mn (atomic fraction) as a view into the grain boundary plane of a region of the grain boundary displayed in (b).

consistently reduced when the temperature is increased. The critical composition is shifted to lower Mn values at higher temperatures due to the asymmetry of the Gibbs energy as a function of the Mn composition and the miscibility gap. Such behaviour has important consequences for the role of Mn segregation during the nucleation of austenite.

6. Segregation in equilibrium with a second stable phase

The calculated values of segregation displayed in Fig. 4 assumed no formation of a second phase. They reasonably describe the segregation behaviour in Fe-Mn alloys prior to and independent of the formation of austenite. Further, they indicate that a high amount of Mn will be available for the formation of austenite via segregation especially above the critical composition of the bulk at which the grain boundary first order transition takes place. Kinetically, the first order grain boundary transition translates into a spinodal-type of segregation which enables formation of the first nucleus of austenite once the fluctuations become strong enough in composition and wavelength. The critical composition of the austenite nucleus will have the same chemical potential as the grain boundary composition and the surrounding bulk composition [64,65]. The austenite nucleus will further grow depleting both the matrix and the grain boundary in solute Mn. Concomitantly, the composition of the austenite decreases until the point where the chemical potential of the austenite is equal to the chemical potential of the BCC bulk phase according to the lever rule (or the composition given by the solvus lines in the phase diagram). The equilibrium amount of segregation in the grain boundary will be the composition at the same chemical potential as the austenite and the BCC bulk phase. Fig. 5 schematically describes the evolution of the composition of the grain boundary using the parallel tangent construction. Fig. 5a shows the metastable equilibrium composition of the grain boundary if austenite would not exist (i.e., the

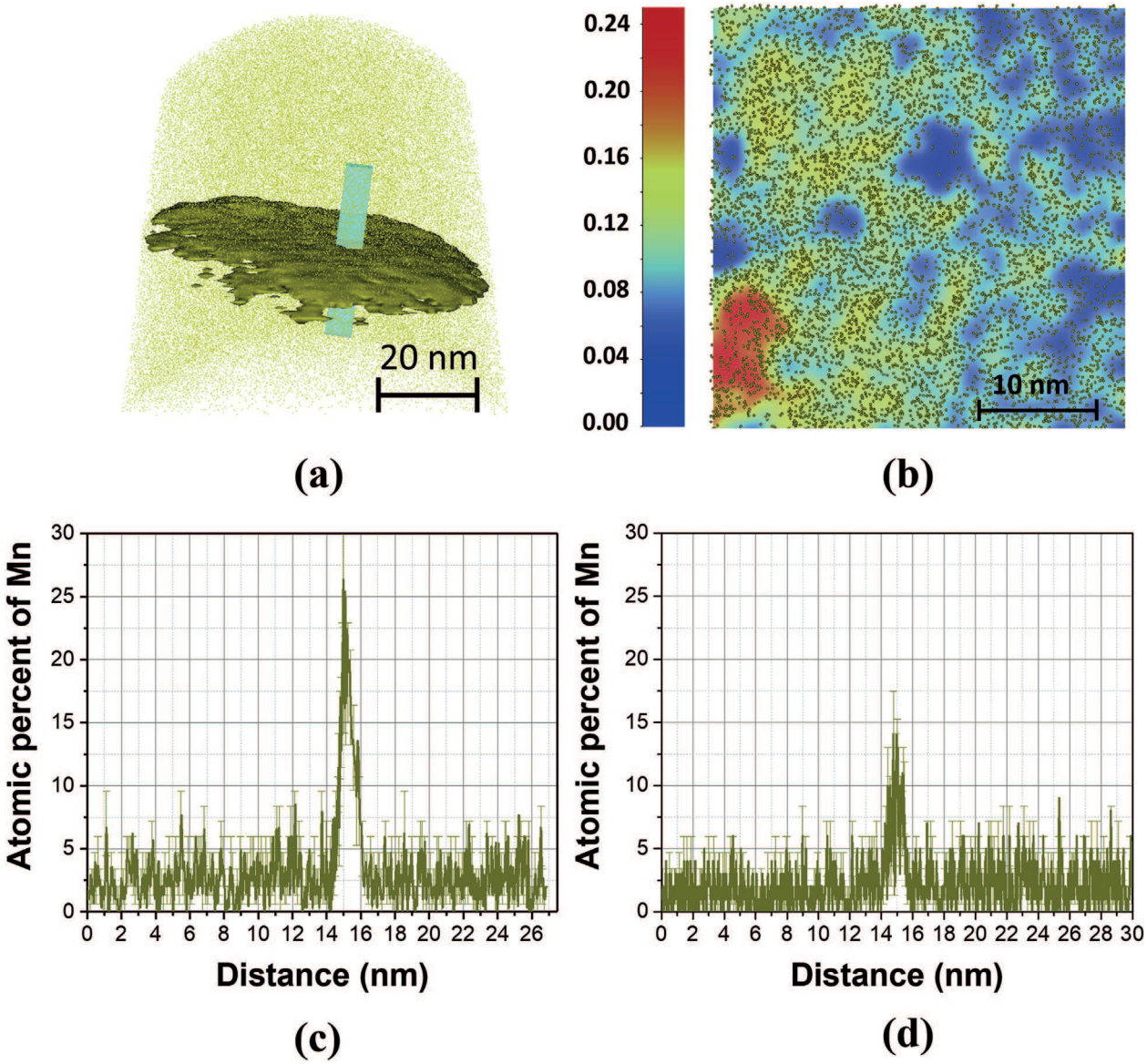

Fig. 7. Fe-4Mn (wt.%) solid solution bulk alloy, 50% cold-rolled and subsequently annealed at 450 °C for 2 months (a) APT reconstruction: 6 at% Mn isosurface revealing a grain boundary at an in-plane view. (b) In-plane 2D compositional map of Mn (atomic fraction) as a view into the grain boundary plane of a region of the grain boundary displayed in (a). (c) and (d) 1D-compositional profile across the grain boundary obtained from different regions of the grain boundary displayed in (a). This composition spread between 25 at% Mn (c) and 14 at% Mn (d) matches the expected segregation state above the critical composition for a first order transition or spinodal segregation.

composition at which $\delta\mu^{\alpha}_{Mn} = \delta\mu^{\alpha,\,GB}_{Mn}$). Fig. 5b and c shows the equilibrium composition of the grain boundary when austenite already exists with the equilibrium composition (i.e., the composition at which $\delta\mu^{\gamma}_{Mn} = \delta\mu^{\alpha}_{Mn} = \delta\mu^{\alpha,\,GB}_{Mn}$).

The segregation of Mn to grain boundaries is a well-known cause of embrittlement in Fe-Mn steels. The cause for the Mn embrittlement can be inferred from the Gibbs energy of mixing of Fe and Mn for the BCC phase showed in Fig. 3a. At a given tempering temperature, Mn will segregate to the grain boundary due to the lower enthalpy of mixing of this element with Fe at the grain boundary. Nevertheless, the mixing enthalpy of Mn and Fe is still positive and the total enthalpy of the boundary is increased by segregating Mn. As a result, when the alloy is cooled down and the atomic mobility is reduced, the grain boundary is 'quenched' into a higher energy state compared to its state before the segregation took place. For compositions above the critical composition for spinodal segregation, the amount of segregation will be remarkably higher than the compositions below this critical composition. Therefore, the increase of the enthalpy of the boundary and the associated embrittlement due to the reduced cohesive energy of the boundary is much higher above the critical composition. This sharp transition is demonstrated schematically in Fig. 5d which shows the mixing energy of the boundary before and after the segregation. The segregation values were calculated using the data shown in Fig. 4. The spinodal segregation at 450 °C leads to an abrupt increase in the energy of the grain boundary at lower temperatures (e.g. 15 °C). When austenite is formed, the total amount of Mn segregated to the grain boundaries as well as the energy of the grain boundary are reduced. The existence of this sharp transition and the increase of toughness due to the formation of austenite were already reported before, e.g. by Kuzmina et al. [26] who revealed this effect in terms of a detailed experimental study combining APT analysis of grain boundary segregation and impact testing.

7. Experimental validation of the existence of a first-order transition of the interface

Extensive APT analysis has been performed for the Fe-9at.%Mn alloy, 50% cold-rolled and subsequently annealed at 450 °C for 6 h, 2 weeks and 2 months, respectively in part as reported in a previous publication [29]. A systematic spatially-confined, i.e. coordination-reduced spinodal-like decomposition behaviour for this alloy was observed both along dislocations and at grain boundaries. The existence of such spinodal fluctuations indicates that the Fe-9at.%Mn alloy composition is above the critical composition for the first order transition shown in the isotherms in Fig. 4. Besides, a large difference has not been observed between the fluctuations at the grain boundaries and at the dislocations. Such behaviour is again consistent with the calculations shown in Fig. 4, since above the critical composition, the interaction between the solutes is stronger than the interaction with sites of different coordination. Consistently, the formation of austenite after extended heat treatments has been reported [26,29]. The austenite at the beginning (6 h and 2 weeks, respectively) of the transformation contains more Mn (around 32 at% Mn) than the austenite in local equilibrium (around 25.5 at% Mn) observed after longer heat treatments. At the same time, after a high volume fraction of austenite is formed, the spinodal segregation is no longer observed which implies that the spinodal segregation and the first order transition of the grain boundary is a metastable state prior to the formation of austenite at the interface. Therefore, the first order transition and the spinodal segregation should not be expected for bulk compositions below the solvus line (single phase region in the phase diagram).

In order to validate the existence of a first order transition of the grain boundary before the austenite nucleation, two additional alloy compositions with 3 and 4 at.% of Mn were studied by APT. Fig. 6a shows the position of these compositions in the binary Fe-Mn phase diagram. This phase diagram includes the metastable miscibility gap and magnetic spinodal of the BCC phase. The Fe9at.%Mn and Fe4at.%Mn alloys are in the two phase field of the phase diagram (ferrite and austenite are stable phases). The Fe3at.%Mn alloy is located in the single phase field of the phase diagram (solid solution ferrite is the only stable phase). Fig. 6b shows an APT reconstruction obtained from an Fe3at.%Mn alloy, 50% cold-rolled and subsequently annealed at 450 °C for 2 months. A grain boundary is highlighted by using a 5 at% Mn isosurface. Fig. 6c shows a composition profile obtained as a function of the distance to the iso-composition surface displayed in Fig. 6b. The average composition of the grain boundary shows a maximum around 8–9 at% Mn, which is consistently below the critical composition for the first order transition shown in Fig. 4a. Small fluctuations are observed at the grain boundary that can be attributed to preferential segregation sites like dislocations (Fig. 6d), but the low magnitude of the fluctuations cannot be considered to be of a spinodal origin. Furthermore, in agreement with the Fe-Mn phase diagram, the formation of austenite was not observed for this alloy.

A combination of APT (for near-atomic scale chemical characterization) and high-resolution electron back scattered diffraction (HR-EBSD, for structural characterization) measurements was performed in an Fe-4at.%Mn alloy, 50% cold-rolled and subsequently annealed at 450 °C for 2 months. This alloy composition is slightly above the solvus line (two phase-region in the phase diagram shown in Fig. 6a). Fig. 7a shows an APT reconstruction revealing a grain boundary. Fig. 7b shows an in-plane 2D compositional map of Mn (atomic fraction) as a view into the grain boundary plane of a region of the grain boundary displayed in 7a. Fig. 7c and d shows the composition of the grain boundary from two different regions: one around 25 at% Mn (Fig. 7c) and the other around 14 at% Mn (Fig. 7d). Such behaviour is again consistent with the expected segregation state above the critical composition for the first order transition or spinodal segregation. More important, it reveals a remarkable non-linear change of the segregation

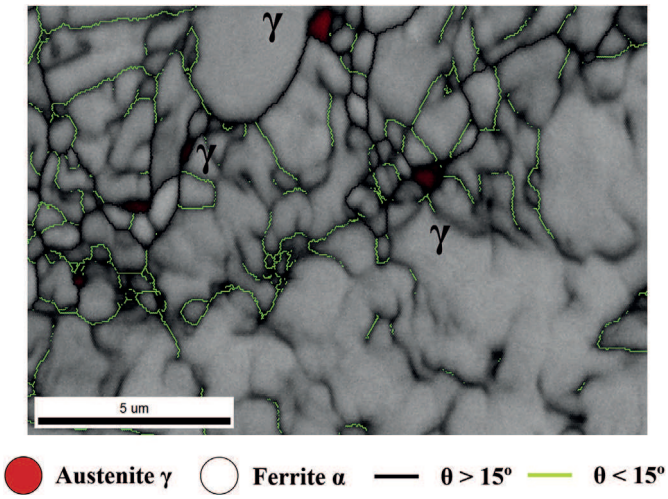

Fig. 8. Fe-4Mn (wt.%) solid solution bulk alloy, 50% cold-rolled and subsequently annealed at 450 °C for 2 months. EBSD map (Image Quality) showing the presence of austenite (in red) in the microstructure after annealing. The green lines indicate low-angle grain boundaries (3–15° of misorientation) and the black lines indicates high-angle grain boundaries (>15° of misorientation).

Table 1
Chemical composition of the Fe4at.%Mn and Fe3at.%Mn alloys in wt.% according to wet-chemical analysis.

Alloy	Mn	C	Ni	Al	S	P	O	N	Fe
Fe4Mn	3.92	0.0081	0.0172	<0.002	0.0036	<0.002	0.0096	0.0071	balance
Fe3Mn	2.95	0.0079	0.0214	<0.001	0.0028	<0.002	0.0196	0.0024	balance

behaviour by increasing the Mn content in the alloy from 3 at% to 4 at% of Mn. This non-linear change of the composition of the grain boundaries with the bulk composition indicates the existence of a first order transition of the grain boundary, as predicted by our model. Fig. 8 displays a phase map obtained by EBSD which confirms that austenite can be formed at this temperature (450 °C) after extended heat treatment (2 months).

8. Conclusions

Grain boundary segregation plays a critical role for a wide range of materials properties and interfacial phase transitions. Limited access to grain boundary thermodynamics, however, has up to now restricted the ability for conducting predictive studies of interfacial segregation and associated decomposition and/or phase states. Here a mean-field model is proposed that links grain boundary thermodynamics to existing thermodynamics data of the corresponding bulk material. The application of the model was exemplified for Fe-Mn binary alloys. The model successfully predicts the existence of a first order transition (or spinodal segregation) of the grain boundary, as experimentally observed by APT. Compositions above a critical value (e.g. Fe9at.%Mn and Fe4at.%Mn) will display spinodal segregation, while compositions below a critical value (e.g. Fe3at.%Mn) will display regular segregation. The spinodal segregation leads to a drastic increase in the enthalpy of the grain boundary and, therefore, to interfacial embrittlement at lower temperatures. Another important consequence of the model is that spinodal segregation provides a non-classical, i.e. chemistry-driven pathway for the heterogeneous nucleation of a second phase (e.g., austenite) and, after growth of this second phase, to the toughening of the grain boundary. Through the change of the local compositional working point via grain boundary segregation, specific spinodal decomposition and chemical precursor states become possible at interfaces that do not occur in the adjacent bulk. Hence, heterogeneous nucleation can proceed both, through providing interfacial energy and by enabling formation of compositional precursors that bring the grain boundary region closer to the composition of stable phases.

9. Materials and methods

9.1. Materials

Two binary Fe-Mn alloys, identified as Fe3at.%Mn and Fe4at.%Mn, were cast into a rectangular billet in a vacuum induction furnace. The slabs were hot-rolled at 1100 °C from 60 to 6 mm thickness and then water quenched. Subsequently, highly segregated edges of the slab were cut off. The billets were reheated to 1100 °C for 1 h and water quenched to room temperature to minimize Mn banding. Table 1 summarizes the chemical composition after homogenization according to wet chemical analysis. After water quenching from the homogenizing temperature the alloys had a fully massive ferrite microstructure. The alloys were subsequently annealed up to 2 months at 450 °C in order to characterize the equilibrium amount of segregation at the grain boundaries. The Fe4at.%Mn alloy is situated in the two phase field of the phase diagram (ferrite and austenite are stable phases). The Fe3at.%Mn alloy is situated in the single phase field of the phase diagram (ferrite is the only stable phase).

9.2. Methods

Atom Probe Tomography (APT) specimens with end radii below 100 nm were prepared using a FEI Helios NanoLab600i dual-beam Focused Ion Beam (FIB)/Scanning Electron Microscopy (SEM) instrument. APT was performed using a LEAP 5000 XS device by Cameca Scientific Instruments, with approx. 80% detection efficiency, at a set-point temperature of 50 K in laser-pulsing mode at a wavelength of 355 nm, 500 kHz pulse repetition rate and 30 pJ pulse energy. For reconstructing 3D atom maps, visualization and quantification of segregation the commercial software IVAS® by Cameca was employed following the protocol introduced by Geiser et al. [66] and detailed in Gault et al. [67]. The 3D-mapping was obtained by the Voltage-based reconstruction of the detected ions. The detector reveals elements of the local crystallography of the sample, allowing for atom probe crystallography analysis of the dataset. The reconstructions were calibrated by the interplanar distance of the crystallographic planes associated with the low-hit density poles. High-resolution electron back-scattered diffraction (HR-EBSD) measurements were performed at a step size of 50 nm using a JEOL JSM-6500F field emission gun scanning electron microscope equipped with a high-speed CCD camera for pattern recording, and analysed using the TSL-OIM software.

Acknowledgements

A. Kwiatkowski da Silva is grateful to the Brazilian National Research Council (Conselho Nacional de Pesquisas, CNPQ) for the PhD scholarship through the “Science without Borders” Project (203077/2014-8). R. Darvishi Kamachali acknowledges the financial supports from the Deutsche Forschungsgemeinschaft (DFG) with the Heisenberg program, project DA 1655/2–1. U. Tezins & A. Sturm are acknowledged for their support to the users of the atom probe facility at MPIE.

References

[1] J.W. Gibbs, Collected Works, Yale University Press, New Haven, Connecticut, 1948.
[2] A.E. Alexander, A.M. Posner, A method of integrating the Gibbs adsorption isotherm, Nature 166 (4219) (1950) 432–433.
[3] R.A. Alberty, On the derivation of the Gibbs Adsorption equation, Langmuir 11 (1995) 3598–3600.
[4] I. Langmuir, The adsorption of gases on plane surfaces of glass, mica and platinum, J. Am. Chem. Soc. 40 (1918) 1361–1403.
[5] D. McLean, Grain Boundaries in Metals, Clarendon Press, Oxford, 1957.
[6] E.D. Hondros, M.R. Seah, S. Hofmann, P. Lejček, Chapter 13 - interfacial and surface microchemistry a2 -, in: Robert W. Cahn, P. Haasen (Eds.), Physical Metallurgy (Fourth, Revised and Enhanced Edition), North-Holland, Oxford, 1996, pp. 1201–1289.
[7] P. Lejcek, Grain Boundary Segregation in Metals, Grain Boundary Segregation in Metals, 2010, pp. 1–239.
[8] R.H. Fowler, E.A. Guggenheim, Statistical Thermodynamics, MacMillan, New York, 1939.
[9] E.W. Hart, 2-dimensional phase transformation in grain boundaries, Scripta Metall. 2 (3) (1968) 179–&.
[10] T.L. Hill, Statistical Mechanics, McGraw-Hill, New York, 1956.
[11] J.H. deBoer, The Dynamical Character of Adsorption, Oxford University Press, London, 1953.
[12] A.R. Miedema, Surface segregation in alloys of transition-metals, Zeitschrift

Fur Metallkunde 69 (7) (1978) 455–461.
[13] E.W. Hart, Grain boundary phase transformations, in: H. Hu (Ed.), The Nature and Behavior of Grain Boundaries: A Symposium Held at the TMS-AIME Fall Meeting in Detroit, Michigan, October 18–19, 1971, Springer US, Boston, MA, 1995, pp. 155–170.
[14] M. Guttmann, P.R. Krahe, F. Abel, G. Amsel, M. Bruneaux, C. Cohen, Temper embrittlement and intergranular segregation of antimony - quantitative-analysis performed with backscattering of energetic ions, Metall. Trans. 5 (1) (1974) 167–177.
[15] M. Guttmann, P. Dumoulin, M. Wayman, The thermodynamics of interactive co-segregation of phosphorus and alloying elements in iron and temper-brittle steels, Metall. Trans. a-Phys. Metall. Mater. Sci. 13 (10) (1982) 1693–1711.
[16] M. Guttmann, Equilibrium segregation in a ternary solution - model for temper embrittlement, Surf. Sci. 53 (DEC) (1975) 213–227.
[17] M. Guttmann, Grain-boundary segregation, 2 dimensional compound formation, and precipitation, Metall. Trans. a-Phys. Metall. Mater. Sci. 8 (9) (1977) 1383–1401.
[18] J.W. Cahn, Transitions and phase-equilibria among grain-boundary structures, J. Phys. 43 (NC-6) (1982) 199–213.
[19] M. Tang, W.C. Carter, R.M. Cannon, Grain boundary transitions in binary alloys, Phys. Rev. Lett. 97 (7) (2006).
[20] W.D. Kaplan, D. Chatain, P. Wynblatt, W.C. Carter, A review of wetting versus adsorption, complexions, and related phenomena: the rosetta stone of wetting, J. Mater. Sci. 48 (17) (2013) 5681–5717.
[21] S.J. Dillon, M. Tang, W.C. Carter, M.P. Harmer, Complexion: a new concept for kinetic engineering in materials science, Acta Mater. 55 (18) (2007) 6208–6218.
[22] P.R. Cantwell, M. Tang, S.J. Dillon, J. Luo, G.S. Rohrer, M.P. Harmer, Grain boundary complexions, Acta Mater. 62 (2014) 1–48.
[23] C. Rottman, Theory of phase-transitions at internal interfaces, J. Phys. 49 (C-5) (1988) 313–326.
[24] Z. Pan, T.J. Rupert, Effect of grain boundary character on segregation-induced structural transitions, Phys. Rev. B 93 (13) (2016) 134113.
[25] D. Raabe, M. Herbig, S. Sandloebes, Y. Li, D. Tytko, M. Kuzmina, D. Ponge, P.P. Choi, Grain boundary segregation engineering in metallic alloys: a pathway to the design of interfaces, Curr. Opin. Solid State Mater. Sci. 18 (4) (2014) 253–261.
[26] M. Kuzmina, D. Ponge, D. Raabe, Grain boundary segregation engineering and austenite reversion turn embrittlement into toughness: example of a 9 wt.% medium Mn steel, Acta Mater. 86 (2015) 182–192.
[27] Z.Y. Yu, P.R. Cantwell, Q. Gao, D. Yin, Y.Y. Zhang, N.X. Zhou, G.S. Rohrer, M. Widom, J. Luo, M.P. Harmer, Segregation-induced ordered superstructures at general grain boundaries in a nickel-bismuth alloy, Science 358 (6359) (2017) 97–+.
[28] R. Kirchheim, B. Somerday, P. Sofronis, Chemomechanical effects on the separation of interfaces occurring during fracture with emphasis on the hydrogen-iron and hydrogen-nickel system, Acta Mater. 99 (2015) 87–98.
[29] A. Kwiatkowski da Silva, D. Ponge, Z. Peng, G. Inden, Y. Lu, A. Breen, B. Gault, D. Raabe, Phase nucleation through confined spinodal fluctuations at crystal defects evidenced in Fe-Mn alloys, Nat. Commun. 9 (1) (2018) 1137.
[30] A. Kwiatkowski da Silva, G. Leyson, M. Kuzmina, D. Ponge, M. Herbig, S. Sandlöbes, B. Gault, J. Neugebauer, D. Raabe, Confined chemical and structural states at dislocations in Fe-9wt%Mn steels: a correlative TEM-atom probe study combined with multiscale modelling, Acta Mater. 124 (2017) 305–315.
[31] A. Kwiatkowski da Silva, G. Inden, A. Kumar, D. Ponge, B. Gault, D. Raabe, Competition between formation of carbides and reversed austenite during tempering of a medium-manganese steel studied by thermodynamic-kinetic simulations and atom probe tomography, Acta Mater.
[32] L. Yuan, D. Ponge, J. Wittig, P. Choi, J.A. Jimenez, D. Raabe, Nanoscale austenite reversion through partitioning, segregation and kinetic freezing: example of a ductile 2 GPa Fe-Cr-C steel, Acta Mater. 60 (6–7) (2012) 2790–2804.
[33] D. Raabe, D. Ponge, M.M. Wang, M. Herbig, M. Belde, H. Springer, Iop, 1 billion tons of nanostructure - segregation engineering enables confined transformation effects at lattice defects in steels, in: 38th Riso International Symposium on Materials Science, 2017.
[34] O. Dmitrieva, D. Ponge, G. Inden, J. Millán, P. Choi, J. Sietsma, D. Raabe, Chemical gradients across phase boundaries between martensite and austenite in steel studied by atom probe tomography and simulation, Acta Mater. 59 (1) (2011) 364–374.
[35] H. Zhao, F. De Geuser, A. Kwiatkowski da Silva, A. Szczepaniak, B. Gault, D. Ponge, D. Raabe, Segregation assisted grain boundary precipitation in a model Al-Zn-Mg-Cu alloy, Acta Mater. 156 (2018) 318–329.
[36] A. Lawrence, J.M. Rickman, M.P. Harmer, A.D. Rollett, Parsing abnormal grain growth, Acta Mater. 103 (2016) 681–687.
[37] R. Kirchheim, Grain coarsening inhibited by solute segregation, Acta Mater. 50 (2) (2002) 413–419.
[38] R. Kirchheim, Reducing grain boundary, dislocation line and vacancy formation energies by solute segregation. I. Theoretical background, Acta Mater. 55 (15) (2007) 5129–5138.
[39] A.R. Kalidindi, T. Chookajorn, C.A. Schuh, Nanocrystalline materials at equilibrium: a thermodynamic review, JOM (J. Occup. Med.) 67 (12) (2015) 2834–2843.
[40] F. Liu, R. Kirchheim, Grain boundary saturation and grain growth, Scripta Mater. 51 (6) (2004) 521–525.
[41] R. Kirchheim, Reducing grain boundary, dislocation line and vacancy formation energies by solute segregation II. Experimental evidence and consequences, Acta Mater. 55 (15) (2007) 5139–5148.
[42] T.J. Rupert, J.C. Trenkle, C.A. Schuh, Enhanced solid solution effects on the strength of nanocrystalline alloys, Acta Mater. 59 (4) (2011) 1619–1631.
[43] T.J. Rupert, The role of complexions in metallic nano-grain stability and deformation, Curr. Opin. Solid State Mater. Sci. 20 (5) (2016) 257–267.
[44] C. Schuh, T. Nieh, H. Iwasaki, The effect of solid solution W additions on the mechanical properties of nanocrystalline Ni, Acta Mater. 51 (2) (2003) 431–443.
[45] A.J. Detor, C.A. Schuh, Grain boundary segregation, chemical ordering and stability of nanocrystalline alloys: atomistic computer simulations in the Ni–W system, Acta Mater. 55 (12) (2007) 4221–4232.
[46] J.R. Trelewicz, C.A. Schuh, Grain boundary segregation and thermodynamically stable binary nanocrystalline alloys, Phys. Rev. B 79 (9) (2009), 094112.
[47] T. Chookajorn, H.A. Murdoch, C.A. Schuh, Design of stable nanocrystalline alloys, Science 337 (6097) (2012) 951–954.
[48] M.A. Gibson, C.A. Schuh, Segregation-induced changes in grain boundary cohesion and embrittlement in binary alloys, Acta Mater. 95 (2015) 145–155.
[49] P. Wynblatt, R.C. Ku, Surface energy and solute strain energy effects in surface segregation, Surf. Sci. 65 (2) (1977) 511–531.
[50] P. Wynblatt, D. Chatain, Anisotropy of segregation at grain boundaries and surfaces, Metall. Mater. Trans. 37 (9) (2006) 2595–2620.
[51] M. Militzer, J. Wieting, Interfacial two-dimensional phase transitions and impurity segregation, Acta Metall. 35 (11) (1987) 2765–2777.
[52] R. DeHoff, Thermodynamics in Materials Science, second ed., Taylor & Francis, 2006.
[53] Interfaces, in: M. Hillert (Ed.), Phase Equilibria, Phase Diagrams and Phase Transformations: Their Thermodynamic Basis, Cambridge University Press, Cambridge, 2007, pp. 344–376.
[54] H. Butt, K. Graf, M. Kappl, Adsorption, Physics and Chemistry of Interfaces, Wiley-VCH, 2004.
[55] M. Methfessel, D. Hennig, M. Scheffler, Calculated surface energies of the 4d transition metals: a study of bond-cutting models, Appl. Phys. A 55 (5) (1992) 442–448.
[56] G. Inden, Determination of chemical and magnetic interchange energies in bcc alloys, Zeitschrift Fur Metallkunde 66 (10) (1975) 577–582.
[57] G. Inden, Determination of chemical and magnetic interchange energies in bcc alloys .3. application to ferromagnetic-alloys, Zeitschrift Fur Metallkunde 68 (8) (1977) 529–534.
[58] G. Inden, The role of magnetism in the calculation of phase diagrams, Phys. B+C 103 (1) (1981) 82–100.
[59] M. Hillert, M. Jarl, A model for alloying in ferromagnetic metals, Calphad 2 (3) (1978) 227–238.
[60] F. Körmann, A.A.H. Breidi, S.L. Dudarev, N. Dupin, G. Ghosh, T. Hickel, P. Korzhavyi, J.A. Muñoz, I. Ohnuma, Lambda transitions in materials science: recent advances in CALPHAD and first-principles modelling, Phys. Status Solidi 251 (1) (2014) 53–80.
[61] N. Saunders, A.P. Miodownik, CALPHAD (Calculation of Phase Diagrams): a Comprehensive Guide, Pergamon, Oxford, 1998.
[62] D. Djurovic, B. Hallstedt, J. von Appen, R. Dronskowski, Thermodynamic assessment of the Fe-Mn-C system, Calphad Comput. Coupling Phase Diagrams Thermochem. 35 (4) (2011) 479–491.
[63] W.M. Huang, An assessment of the Fe-Mn system, Calphad Comput. Coupling Phase Diagrams Thermochem. 13 (3) (1989) 243–252.
[64] H.I. Aaronson, M. Enomoto, J.K. Lee, Mechanisms of Diffusional Phase Transformations in Metals and Alloys, 2010.
[65] I.R.S. Filho, A. Kwiatkowski da Silva, M.J.R. Sandim, D. Ponge, B. Gault, H.R.Z. Sandim, D. Raabe, Martensite to austenite reversion in a high-Mn steel: partitioning-dependent two-stage kinetics revealed by atom probe tomography, in-situ magnetic measurements and simulation, Acta Mater. 166 (2019) 178–191.
[66] B.P. Geiser, D.J. Larson, E. Oltman, S. Gerstl, D. Reinhard, T.F. Kelly, T.J. Prosa, Wide-Field-of-View atom probe reconstruction, Microsc. Microanal. 15 (2009) 292–293.
[67] B. Gault, D. Haley, F. de Geuser, M.P. Moody, E.A. Marquis, D.J. Larson, B.P. Geiser, Advances in the reconstruction of atom probe tomography data, Ultramicroscopy 111 (6) (2011) 448–457.
[68] N. Ma, S.A. Dregia, Y. Wang, Solute segregation transition and drag force on grain boundaries, Acta. Mater. 51 (13) (2003) 3687–3700.